Redox Biology 18 (2018) 124–137

Contents lists available at ScienceDirect

Redox Biology

journal homepage: www.elsevier.com/locate/redox

Research Paper

Polydatin prevents fructose-induced liver inflammation and lipid deposition through increasing miR-200a to regulate Keap1/Nrf2 pathway

Xiao-Juan Zhao, Han-Wen Yu, Yan-Zi Yang, Wen-Yuan Wu, Tian-Yu Chen, Ke-Ke Jia, Lin-Lin Kang, Rui-Qing Jiao, Ling-Dong Kong*

State Key Laboratory of Pharmaceutical Biotechnology, School of Life Sciences, Nanjing University, Nanjing 210023, PR China

ARTICLE INFO

Keywords:
Polydatin
Excess fructose intake
Oxidative stress
MiR-200a
Keap1/Nrf2 pathway
Liver inflammation and lipid deposition

ABSTRACT

Oxidative stress is a critical factor in nonalcoholic fatty liver disease pathogenesis. MicroRNA-200a (miR-200a) is reported to target Kelch-like ECH-associated protein 1 (Keap1), which regulates nuclear factor erythroid 2-related factor 2 (Nrf2) anti-oxidant pathway. Polydatin (3,4′,5-trihydroxy-stilbene-3-β-D-glucoside), a polyphenol found in the rhizome of *Polygonum cuspidatum*, have anti-oxidative, anti-inflammatory and anti-hyperlipidemic effects. However, whether miR-200a controls Keap1/Nrf2 pathway in fructose-induced liver inflammation and lipid deposition and the blockade of polydatin are still not clear. Here, we detected miR-200a down-regulation, Keap1 up-regulation, Nrf2 antioxidant pathway inactivation, ROS-driven thioredoxin-interacting protein (TXNIP) over-expression, NOD-like receptor (NLR) family, pyrin domain containing 3 (NLRP3) inflammasome activation and dysregulation of peroxisome proliferator activated receptor-α (PPAR-α), carnitine palmitoyl transferase-1 (CPT-1), sterol regulatory element binging protein 1 (SREBP-1) and stearoyl-CoA desaturase-1 (SCD-1) in rat livers, BRL-3A and HepG2 cells under high fructose induction. Furthermore, the data from the treatment or transfection of miR-200a minic, *Keap1* and *TXNIP* siRNA, Nrf2 activator and ROS inhibitor demonstrated that fructose-induced miR-200a low-expression increased Keap1 to block Nrf2 antioxidant pathway, and then enhanced ROS-driven TXNIP to activate NLRP3 inflammasome and disturb lipid metabolism-related proteins, causing inflammation and lipid deposition in BRL-3A cells. We also found that polydatin up-regulated miR-200a to inhibit Keap1 and activate Nrf2 antioxidant pathway, resulting in attenuation of these disturbances in these animal and cell models. These findings provide a novel pathological mechanism of fructose-induced redox status imbalance and suggest that the enhancement of miR-200a to control Keap1/Nrf2 pathway by polydatin is a therapeutic strategy for fructose-associated liver inflammation and lipid deposition.

1. Introduction

Clinical and experimental evidences demonstrate that excessive fructose consumption causes nonalcoholic fatty liver disease pathogenesis [1,2]. Oxidative stress is considered to be a critical factor in this pathogenesis [3]. However, the mechanisms of fructose-induced redox status imbalance in liver inflammation and lipid accumulation are still poorly elucidated. Kelch-like ECH-associated protein 1 (Keap1) directly leads to continual ubiquitination and subsequent degradation of the transcription factor nuclear factor (erythroid-derived 2)-like 2 (Nrf2) in cell cytoplasm [4]. Upon dissociated from Keap1, Nrf2 is translocated into nuclear, and then initiates phase II detoxification and antioxidant defense enzyme to counteract oxidative stress and modulate redox status balance [5]. Keap1 ablation increases Nrf2 nuclear translocation and up-regulates hemeoxygenase-1 (HO-1), attenuates palmitate-induced reactive oxygen species (ROS) production in human hepatoblastoma cell line (HepG2) [6]. Nrf2 knockout develops thioredoxin-interacting protein (TXNIP) and nucleotide-binding domain (NOD)-like

Abbreviations: ASC, apoptosis-associated speck-like protein; CPT-1, carnitine palmitoyl transferase-1; GST, glutathione S-transferase; HO-1, hemeoxygenase-1; H2O2, hydrogen peroxide; IL, interleukin; Keap1, Kelch-like ECH-associated protein 1; MDA, malondialdehyde; miR-200a, microRNA-200a; NAC, N-acetyl-L-cysteine; NAFLD, non-alcoholic fatty liver disease; NLRP3, the NOD-like receptor (NLR) family, pyrin domain containing 3; NQO1, NAD(P)H, quinone oxidoreductase 1; Nrf2, nuclear factor erythroid 2-related factor 2; PPAR-α, peroxisome proliferator activated receptor-α; ROS, reactive oxygen species; SCD-1, stearoyl-CoA desaturase-1; SREBP-1, sterol regulatory element binging protein 1; tBHQ, *tert*-butylhydroquinone; TNF-α, tumor necrosis factor-α; TXNIP, thioredoxin-interacting protein

* Correspondence to: State Key Laboratory of Pharmaceutical Biotechnology, Nanjing University, Nanjing 210023, PR China.
E-mail address: kongld@nju.edu.cn (L.-D. Kong).

https://doi.org/10.1016/j.redox.2018.07.002
Received 20 June 2018; Received in revised form 1 July 2018; Accepted 4 July 2018
Available online 05 July 2018

receptor protein 3 (NLRP3) high-expression in lipopolysaccharide (LPS)-induced lung inflammation of mice [7]. TXNIP can activate nucleotide-binding domain (NOD)-like receptor protein 3 (NLRP3) inflammasome and subsequently generate interlin-1β (IL-1β) in response to oxidative stress [8]. Nrf2 activation simulated by *tert*-butylhydroquinone (tBHQ) increases NAD(P)H: quinone oxidoreductase 1 (NQO1) to scavenge ROS, this process inhibits NLRP3 inflammasome activation and IL-1β production in adenosine triphosphate and lipopolysaccharide-exposed human THP-1 cell- and bone marrow-derived macrophages [9]. Thus, anti-oxidation function of the Nrf2 pathway may contribute to the elimination of ROS and subsequent inflammatory response [10]. Specific Keap1 knockout blocks ethanol-inducted increase of liver triglyceride (TG) levels and up-regulation of sterol regulatory element-binding protein 1 (SREBP-1) and its target gene stearoyl-CoA desaturase 1 (SCD-1) in Nrf2-null mice [11]. Our previous study showed that ROS-induced TXNIP drove fructose-mediated hepatic inflammation and lipid deposition through NLRP3 inflammasome activation [2]. However, it remains unclear whether and how Keap1/Nrf2 pathway interferes with this event.

There is crosstalk between oxidative stress and microRNA-200a (miR-200a). MiR-200a high-expression by targeting Keap1 inhibition up-regulates Nrf2 nuclear translocation as well as glutathione S-transferase (GST), hemeoxygenase-1 (HO-1) and NQO1 protein levels, and then decreases ROS production in human adult cardiomyocyte line exposed to hypoxia [12], and increases tumor necrosis factor-α (TNF-α) and IL-6 at mRNA levels, as well as down-regulates peroxisome proliferator activated receptor-α (PPAR-α), and up-regulates SCD1 and SREBP-1c at protein levels in fructose-exposed HepG2 cells [13]. It is attractive therefore to hypothesize that aberrant miR-200a expression may target to Keap1 and then inhibit Nrf2 antioxidant pathway, participating in fructose-induced liver inflammation and lipid deposition.

Anti-oxidant agent polydatin (3,4′,5-trihydroxy-stilbene-3-β-D-glucoside), a natural precursor of resveratrol, is isolated from *Polygonum cuspidatum* Siebold & Zucc, which has been used in traditional Chinese medicine to treat liver disorders associated with oxidative stress, inflammation and lipid deposition for centuries in patients [14] and in experimental animals [15,16]. Polydatin decreases malondialdehyde (MDA) levels and increases GST activity in the liver of carbon tetrachloride- or D-galactose-stimulated mice, with the reduction of TNF-α and IL-1β gene expression [17,18]. It inhibits Keap1, promotes Nrf2 transcriptional activity, increases HO-1 protein levels, and quenches ROS generation in advanced glycation-end products-simulated rat glomerular mesangial cells [19]. Additionally, polydatin suppresses kidney NLRP3 inflammasome activation in potassium oxonate-treated rats [20], increases liver PPAR-α protein levels in streptozocin-induced diabetic mice fed with high-fat and sugar diet [21], and decreases liver SCD-1 protein levels in high-fat diet-fed rats [22]. Thus, it is important to understand the molecular mechanism underlying its attenuation of fructose-induced redox status imbalance in liver inflammation and lipid deposition.

In this study, we showed that high fructose decreased miR-200a to target Keap1 and inhibit Nrf2 antioxidant pathway, and then triggered TXNIP-activated NLRP3 inflammasome, causing liver inflammation and lipid deposition. Furthermore, polydatin reduced oxidative stress by increasing miR-200a to regulate Keap1/Nrf2 pathway, resulting in the protection against fructose-induced liver inflammation and lipid deposition. Therefore, the ability of high miR-200a expression to control Keap1/Nrf2 pathway by polydatin may be a new therapeutic strategy.

2. Materials and methods

Reagents For animal experiments, fructose was provided from Shandong Xiwang Sager Industry Co., Ltd. (Binzhou, China), polydatin (purity ≥ 98%) was obtained from Nanjing Spring & Autumn Biological Engineering Co., Ltd. (Nanjing, China), and pioglitazone table was purchased from Jiangsu DeYuan Pharmaceutical Co., Ltd. (Lianyungang, China). For cell experiments, fructose, polydatin, pioglitazone, tBHQ, *N*-acetyl-L-cysteine (NAC) and 2′ 7′-dichlorodihydrofluorescein diacetate ($DCFH_2$-DA) were purchased from Sigma-Aldrich Inc. (St. Louis, MO). Kits of TG, total cholesterol (TC), MDA, hydrogen peroxide (H_2O_2) as well as enzyme-linked immunosorbent assay (ELISA) kits of IL-1β and TNF-α were purchased from Jiancheng Biotechnology Co., Ltd (Nanjing, China), respectively. Kits of nuclear protein and cytoplasmic protein extraction were obtained from Keygen Biotechnology Corp., Ltd (Nanjing, China). Fetal bovine serum was purchased from Wisent Technology (St-Bruno, QC, Canada). DMEM and opti-MEM were purchased from Basal Media Biotechnology Co., Ltd (Shanghai, China). Lipofectamine 2000 was got from Invitrogen Corporation (Carlsbad, CA, USA). Dual-luciferase reporter assay system kit was purchased from Promega Corporation (Madison, USA). Trizol reagent was got from Sigma-Aldrich Inc. (St. Louis, MO). Reverse Transcription System Kit, dNTPs and RNase inhibitor were obtained from Vazyme Biotechnology Co., Ltd (Nanjing, China), respectively. iTaqTM Universal SYBR® Green Supermix was got from Bio-Rad Inc. (California, USA). MultiScribe reverse transcriptase was obtained from Promega Corporation (Wisconsin, USA). Cell lysis buffer was purchased from Beyotime Biotechnology (Nanjing, China, P0013). Pierce™ BCA protein assay kit was purchased from Thermo Scientific (Schwerte, Germany). Rabbit anti-Nrf2 (sc-722), mouse anti-HO-1 (sc-136960), mouse anti-TXNIP (sc-2712138), rabbit anti-ASC (sc-22514), rabbit anti-Caspase-1 (sc-514), rabbit anti-pro-Caspase-1 (sc-514), rabbit anti-PPAR-α (sc-9000), rabbit anti-CPT-1 (sc-139480), rabbit anti-SREBP-1 (sc-367), rabbit anti-SCD-1 (sc-14720) and rabbit anti-GAPDH (sc-25778) were purchased from Santa Cruz Biotechnology Co., Ltd (Santa Cruz, CA, USA). Rabbit anti-Keap1 (#8047), mouse anti-Lamin A/C (#4777), rabbit anti-GST (#2625), mouse anti-NQO1 (#3187), rabbit anti-NLRP3 (#13158) and HRP-conjugated rabbit anti-IgG (#AP132P) were obtained from Cell Signaling Technology (Cambridge, USA). Mouse anti-IL-1β (MAB5011), mouse anti-pro-IL-1β (MAB5011) and HRP-conjugated mouse anti-IgG (HAF007) were got from R&D System (Minneapolis, USA). Mouse anti-β-actin (ABM-0001) was purchased from Zoonbio Biotechnology Co. Ltd. (Nanjing, China).

2.1. Animals and treatment

Male Sprague-Dawley rats aged from 6 to 7 weeks (180–220 g) were purchased from Experimental Animal Center of Zhejiang province (Hangzhou, China) (Production license: SCXK 2014-0001). They were housed in Laboratory Animal Care of Life Science College under controlled temperature (22 ± 2 °C) and relative humidity (55 ± 5%) with a normal 12-h light/dark cycle. Animal welfare and experimental procedures were carried out in accordance with the criteria outlined in the 'Guide for the Care and Use of Laboratory Animals' enacted by National Academy of Sciences and published by the National Institutes of Health (NIH publication 86-23 revised 1985) and the related ethnical regulations of Nanjing University [SYXK (SU) 2009-0017]. All animal experimental protocols were approved by the Institutional Animal Care and Use Committee of Nanjing University. All efforts were made to minimize animal suffering and to reduce the number of animals used.

Rats *ad libitum* accessed a standard chow and water for one week acclimatization before the experiment. To evaluate the protection of polydatin and pioglitazone in fructose-induced liver oxidative stress, inflammation and lipid deposition, rats were randomized into the following six groups (n = 8): control vehicle, fructose vehicle, fructose with polydatin (7.5, 15, 30 mg/kg) as well as fructose with pioglitazone (positive drug, 4 mg/kg). Each rat was given drinking water or 100 mL drinking water containing 10% fructose (wt/vol) for 6 weeks, and followed by the treatment of saline injection, polydatin, or pioglitazone table by intragastric administration for next 7 weeks. All drugs were administered once daily between 2:30 p.m. and 3:30 p.m.. Animal body weight was detected weekly. Doses of polydatin and pioglitazone were selected based on our preliminary studies and other reports [22–27].

Polydatin significantly decreases liver TG, TC and TNF-α levels, as well as down-regulates SREBP-1c and SCD1 protein levels in SD rats with NAFLD at 30 mg/kg [22], decreases kidney IL-1β and TNF-α levels in fructose-fed mice at 12.5, 25 and 50 mg/kg (equivalent 8.75, 17.5, 35 mg/kg to rat) [23]. Pioglitazone is clinically used to improve liver steatosis and inflammation in patients with NAFLD [24–26]. Our previous study showed that pioglitazone at 4 mg/kg significantly alleviated hepatic inflammation and lipid deposition in fructose-fed rats [27]. Therefore, doses of 7.5, 15, and 30 mg/kg polydatin as well as 4 mg/kg pioglitazone were used in these animal experiments.

2.2. Histological study

Light microscopy and histological examination of tissue sections stained with H&E reagent and oil-red O solution were carried out to evaluate whether high fructose intake induced liver inflammation and lipid deposition, and the effects of polydatin and pioglitazone on these pathological changes in rats.

2.3. Cell culture and treatment

Cell lines of Buffalo rat liver cells (BRL-3A) and HepG2 were supported by Shanghai Institutes for Biological Sciences (Shanghai, China). These cells were grown in DMEM (4.5 mg/mL glucose), supplemented with 10% fetal bovine serum in a humidified 5% CO_2 atmosphere at 37 °C, respectively.

During experiments, the cells were plated in 6-, 12- or 96-well plates for 12 h, respectively. The cells were adhered to the walls and made quiescent by incubation in serum-free DMEM for 12 h and then maintained in DMEM with 10% fetal bovine serum. BRL-3A and HepG2 cells were maintained in DMEM and exposed to 0.1% dimethyl sulphoxide alone (control-vehicle), 5 mM fructose (fructose-vehicle), 5 mM fructose co-incubated with 10, 20 and 40 μM polydatin or 10 μM pioglitazone in 6-well plates for 24 h (2 mL/well, 1.0×10^5 cells/mL for BRL-3A cells and 2.0×10^5 cells/mL for HepG2 cells) to determine Keap1, total and nuclear Nrf2, GST, HO-1 and NQO1 protein levels, for 48 h (2 mL/well, 8.0×10^4 cells/mL for BRL-3A cells and 1.0×10^5 cells/mL for HepG2 cells) to detect TXNIP, NLRP3, ASC, Caspase-1, IL-1β, PPAR-α, CPT-1, SREBP-1 and SCD-1 protein levels by Western blot analysis; in 12-well plates (1 mL/well, 1.0×10^6 cells/mL) to analyze miR-200a expression levels (BRL-3A cells: 4 h; HepG2 cells: 12 h), for 24 h (1 mL/well, 5.0×10^5 cells/mL for BRL-3A cells and 5×10^5 mL/well for HepG2 cells) to detect Keap1 mRNA levels, and for 48 h (1 mL/well, 1.0×10^5 cells/mL for BRL-3A cells and 2.0×10^5 mL/well for HepG2 cells) to test TXNIP mRNA levels by qRT-PCR assay; in 96-well plates (200 μL/well, 1.0×10^5cells/mL for BRL-3A cells and 2.0×10^5 cells/mL for HepG2 cells) for 24 h to detect ROS levels by labeling $DCFH_2$-DA; for 48 h (200 μL/well, 5.0×10^4 cells/mL for BRL-3Acells and 1.0×10^5 cells/mL for HepG2 cells) to assay cultural supernatant IL-1β levels by ELISA and test TG and TC levels with standard diagnostic kits, respectively. The selected concentrations and incubation time of these reagents were referred to preliminary experiments and other report [27].

MiR-200a mimic, *Keap1* siRNA, *TXNIP* siRNA as well as these respective negative controls were synthesized by GenePharma Co., Ltd (Shanghai, China), respectively. The sequences of these oligonucleotide fragments were listed in Supplementary Table 2. Transient transfection of 50 nM miR-200a mimic, 50 nM *Keap1* siRNA, 50 nM *TXNIP* siRNA, or respective negative controls was performed using Lipofectamine 2000 following the manufacturer's protocols in BRL-3A cells for 6 h, respectively. These cells were then incubated in opti-MEM for other 18 h. qRT-PCR analysis of miR-200a, Keap1 and TXNIP expression levels and Western blot analysis of Keap1 and TXNIP protein levels were used to confirm the successful transfection, respectively. Then, miR-200a mimic or *Keap1* siRNA-transfected BRL-3A cells were incubated with 5 mM fructose in the presence or absence of 40 μM polydatin or 10 μM pioglitazone in 6-well plates for 24 h to analyze Keap1, nuclear Nrf2, GST, HO-1 and NQO1 protein levels, for 48 h to detect TXNIP, NLRP3, ASC, Caspase-1, IL-1β, PPAR-α, CPT-1, SREBP-1 and SCD-1 protein levels by Western blot analysis; in 96-well plates for 24 h to detect ROS levels by labeling $DCFH_2$-DA; for 48 h to assay TG and TC levels with standard diagnostic kits. BRL-3A cells were pretreated with 10 μM tBHQ (an activator of Nrf2) for 8 h, then incubated with 5 mM fructose in the presence or absence of 40 μM polydatin or 10 μM pioglitazone in 6-well plates for 24 h to analyze Keap1, nuclear Nrf2, GST, HO-1 and NQO1 protein levels, for 48 h to detect TXNIP, NLRP3, ASC, Caspase-1, IL-1β, PPAR-α, CPT-1, SREBP-1 and SCD-1 protein levels by Western blot analysis; in 96-well plates for 24 h to detect ROS levels by labeling $DCFH_2$-DA; for 48 h to assay TG and TC levels with standard diagnostic kits. BRL-3A cells were co-cultured with 5 mM fructose and 5 mM NAC (ROS inhibitor) in the presence or absence of 40 μM polydatin or 10 μM pioglitazone in 6-well plates for 48 h to detect TXNIP protein levels by Western blot analysis. *TXNIP* siRNA-transfected BRL-3A cells were incubated with 5 mM fructose in the presence or absence of 40 μM polydatin or 10 μM pioglitazone in 6-well plates for 24 h to analyze nuclear Nrf2 protein levels, for 48 h to detect TXNIP, NLRP3, ASC, Caspase-1, IL-1β, PPAR-α, CPT-1, SREBP-1 and SCD-1 protein levels by Western blot analysis; in 96-well plates for 24 h to detect ROS levels by labeling $DCFH_2$-DA; for 48 h to assay TG and TC levels with standard diagnostic kits, respectively.

Total cellular proteins, cytoplasm proteins, nuclear proteins and total RNAs were extracted, respectively. Experiments were repeated at least three times. These samples were stored at − 80 °C before biochemical, qTR-PCR and Western blot analysis, respectively.

2.4. Determination of biochemical parameters

For IL-1β, TNF-α, MDA and H_2O_2 assay, rat liver tissue samples were homogenized on ice in saline solution and then centrifuged at $2500 \times g$ for 10 min at 4 °C to get the supernatants. IL-1β and TNF-α levels in liver tissue supernatant or BRL-3A and HepG2 cells cultural supernatant were quantitated by ELISA kits, according to the instructions, respectively. MDA and H_2O_2 levels in liver tissue supernatant were measured with commercial kits, respectively. For TG and TC assay, rat liver tissue samples were homogenized on ice in chloroform/methanol (2:1) and then centrifuged at $2500 \times g$ for 10 min at 4 °C to get the supernatants. BRL-3A and HepG2 cells were lysed on ice in 2% Triton X-100 solution for 40 min followed by centrifugalization at $2500 \times g$ for 10 min at 4 °C to get the supernatants. TG and TC levels in liver tissue supernatant or cell lysate were determined with standard diagnostic kits, respectively. The protein contents of these samples were detected with BCA kit and normalized to the data of biochemical parameters.

2.5. ROS assay

ROS levels in liver tissue were detected with the fluorescence probe 2′ 7′-dichlorodihydrofluorescein diacetate (**$DCFH_2$-DA**). For ROS assay, liver tissue was homogenized in saline solution and centrifuged $10{,}000 \times g$ for 15 min at 4 °C to get the supernatants. Five micromole probe DCFH2-DA (dissolved in PBS) was added into the supernatants at 37 °C for 20 min. Fluorescence was measured at λ_{ex} = 488 nM and λ_{em} = 525 nm with a microplate reader (Thermo Scientific, Schwerte, Germany). The protein contents of liver samples were detected with BCA protein assay kit and normalized to the data of ROS levels.

Intracellular ROS levels in BRL-3A and HepG2 cells were quantified with the fluorescence probe $DCFH_2$-DA. These cell samples were co-cultured in DMEM without fetal bovine serum containing 5 μM $DCFH_2$-DA at 37 °C for 20 min. After washing with 0.01 M phosphate-buffered saline, fluorescence was detected at λ_{ex} = 488 nM and λ_{em} = 525 nm with a microplate reader. Then, these cell samples were exposed to 5 mg/mL 3-(4,5-dimethyl-2-thiazolyl)-2,5-diphenyl-2-H-tetrazolium

Table 1
Effects of polydatin and pioglitazone on liver parameters in fructose-fed rats.

Group	Control +	Fructose +		Fructose + polydatin		Fructose + pioglitazone	
	Vehicle	Vehicle	7.5	15	30	4	mg/kg
IL-1β (ng/g protein)	0.10 ± 0.03	0.17 ± 0.07$^{\#\#\#}$	0.15 ± 0.08	0.15 ± 0.11	0.14 ± 0.11*	0.14 ± 0.11*	
TNF-α (ng/g protein)	4.0 ± 0.2	7.5 ± 0.4$^{\#\#\#}$	6.6 ± 0.6	7.2 ± 0.3	6.1 ± 0.2*	5.9 ± 0.4*	
TG (mmol/g protein)	102 ± 6	207 ± 14$^{\#\#\#}$	118 ± 12***	75 ± 4***	76 ± 6***	96 ± 8***	
TC (mmol/g protein)	37.2 ± 1.6	56.2 ± 3.0$^{\#\#\#}$	47.1 ± 5.5	31.1 ± 2.4***	32.1 ± 1.7***	32.2 ± 2.0***	
ROS (Intensity•mL/mg protein)	81 ± 4	118 ± 5$^{\#\#}$	109 ± 8	97 ± 12	91 ± 8*	91 ± 8*	

Data are expressed as the mean ± S.E.M.. (n = 6 at least). $^{\#\#}P < 0.01$, $^{\#\#\#}P < 0.001$ compared with control-vehicle, $^{*}P < 0.05$, $^{***}P < 0.001$ compared with fructose-vehicle. IL-1β, interleukin-1β; TNF-α, tumor necrosis factor-α; TG, triglyceride; TC, total cholesterol; ROS, reactive oxygen species.

bromide (MTT) solution at 37 °C for another 4 h. After centrifugalization at 2500 × *g* for 5 min at 4 °C to remove supernatant, dimethyl sulphoxide was added to dissolve the precipitation. Absorbance at 570 nm was read on a plate reader. Cell activity was calculated and normalized to the data of ROS levels in BRL-3A and HepG2 cells.

2.6. Dual luciferase reporter assay

Wild-type or mutant of 3′UTR sequences of human Keap1 domain was cloned into the GP-miRGL0 control vector, with the primers listed in Supplementary Table 2. For the luciferase reporter assay, BRL-3A and HepG2 cells were co-transfected with 50 nM negative control or 50 nM of miR-200a mimic and 350 ng of wild-type of GP-miRGL0-Keap1-3′UTR vector. Simultaneously, BRL-3A and HepG2 cells were co-transfected with 50 nM negative control or 50 nM of miR-200a mimic and 350 ng of mutant-type of GP-miRGL0-Keap1-3′UTR vector. After 24 h transfection, cells were harvested. Firefly and Renilla luciferase activity was detected using Dual-luciferase Reporter Assay System kit according to the manufacturer's protocol.

2.7. qRT-PCR

Total RNA, from either frozen liver tissue or cultured cells, was extracted using Trizol reagent according to the instruction of the manufacture. First-strand complementary DNA synthesis for Keap1 and TXNIP were synthesized using the Reverse Transcription System Kit according to the manufacturer's instructions. Gene expression was quantified using iTaqTM Universal SYBR® Green Supermix and gene-specific primers listed in Supplementary Table 2. Expression of Keap1 and TXNIP were normalized to that of the housekeeping genes β-actin. The reverse transcription reactions of miR-200a was performed using 200 ng of purified total RNA, 0.75 μL of stem-loop RT primers listed in Supplementary Table 2, 2 μL of RT buffer, 1 μL of 80 U/μL MultiScribe reverse transcriptase, 1 μL of 10 mM dNTPs, 0.25 μL of 40 U/μL RNase inhibitor, and H_2O-DEPC to 10 μL. The reaction mix was incubated for 15 min at 16 °C, 1 h at 37 °C, 5 min at 85 °C, and then held at 4 °C. The qRT-PCR analyses of miR-200a was carried out with iTaqTM Universal SYBR® Green Supermix and gene-specific primers listed in Supplementary Table 2. Expression of miR-200a was normalized to the levels of U6. The ratio of the relative expression of target genes to the housekeeping genes was calculated by the $2^{-\Delta\Delta T}$ method. All reactions were performed in triplicates for each sample.

2.8. Western blot analysis

Western blot analysis was used to test protein expression levels. In brief, extracts from liver tissues and cultured cells were resolved by SDS-PAGE, transferred to polyvinylidene fluoridemembranes, and then immunoblotted using specific primary antibodies including rabbit anti-Keap1 (dilution 1:1000), anti-Nrf2 (dilution 1:500), rabbit GST (dilution 1:1000), mouse anti-HO-1 (dilution 1:800), mouse anti-NQO1 (dilution 1:1000), mouse anti-TXNIP (dilution 1:800), rabbit anti-NLRP3 (dilution 1:1000), rabbit anti-ASC (dilution 1:800), rabbit anti-Caspase-1 (dilution 1:500), rabbit anti-pro-Caspase-1 (dilution 1:500), mouse anti-IL-1β (dilution 1:1000), mouse anti-pro- IL-1β (dilution 1:1000), rabbit PPAR-α (dilution 1:800), rabbit anti-CPT-1 (dilution 1:800), rabbit anti-SREBP-1 (dilution 1:1000), rabbit anti-SCD-1 (dilution 1:1000), rabbit anti-GAPDH (dilution 1:2000), mouse anti-β-actin (dilution 1:5000), followed by HRP-conjugated anti-rabbit IgG antibody (dilution 1:20000), or HRP-conjugated anti-mouse IgG antibody (dilution 1:2000). Immunoreactive bands were visualized via enhanced chemiluminescence (Cell Signaling Technology) and quantified via densitometry using ImageJ (version 1.42q, National Institutes of Health).

2.9. Statistical analysis

Data are expressed as mean ± S.E.M.. One-way analysis of variance was used for comparison among the different groups, further analyzed by post hoc Dannelt testing. $P < 0.05$ was considered significant. Figures were obtained by the Statistical Analysis System (GraphPad Prism 5, GraphPad Software, Inc., San Diego, CA).

3. Results

3.1. Polydatin alleviates hepatic oxidative stress, inflammation and lipid deposition in vivo and in vitro

In this study, polydatin reduced ROS (Table 1), MDA and H_2O_2 levels (Supplementary Table 1), and down-regulated TXNIP mRNA and protein levels (Fig. 1A and B) in the liver of fructose-fed rats. It also restored fructose feeding-induced inflammatory cells infiltrated in portal area of livers (Fig. 1C), high levels of IL-1β and TNF-α (Table 1) in rats. Consistently, polydatin down-regulated NLRP3, ASC and Caspase-1 protein levels as well as reduced IL-1β production in the liver of fructose-fed rats (Fig. 1D). Additionally, polydatin abrogated liver slight steatosis (Fig. 1C), increased PPAR-α and CPT-1 protein levels, decreased SREBP-1 and SCD-1 protein levels (Fig. 1D), and reduced TG and TC levels (Table 1) in the liver of fructose-fed rats. Pioglitazone exerted the similar effects in this animal model (Fig. 1 and Table 1), except SREBP1 and ASC protein levels.

Next, in fructose-exposed BRL-3A and HepG2 cells, polydatin was found to reduce ROS over-production (24 h) (Fig. 2A) and TXNIP over-expression (48 h) (Fig. 2B, C). Consistently, It decreased NLRP3, ASC, Caspase-1 and IL-1β protein levels, and IL-1β secretion, as well as up-regulated PPAR-α and CPT-1 protein levels, and down-regulated SREBP-1 and SCD-1 protein levels (Fig. 2D–F) with the reduction of TG and TC levels in these cell models (Fig. 2G) (48 h). Pioglitazone had the similar effects in these cell models (Fig. 2), but it failed to change PPAR-α levels induced by fructose. Taken together, these findings support the notion that polydatin and pioglitazone attenuate fructose-induced hepatic oxidative stress, inflammation and lipid deposition.

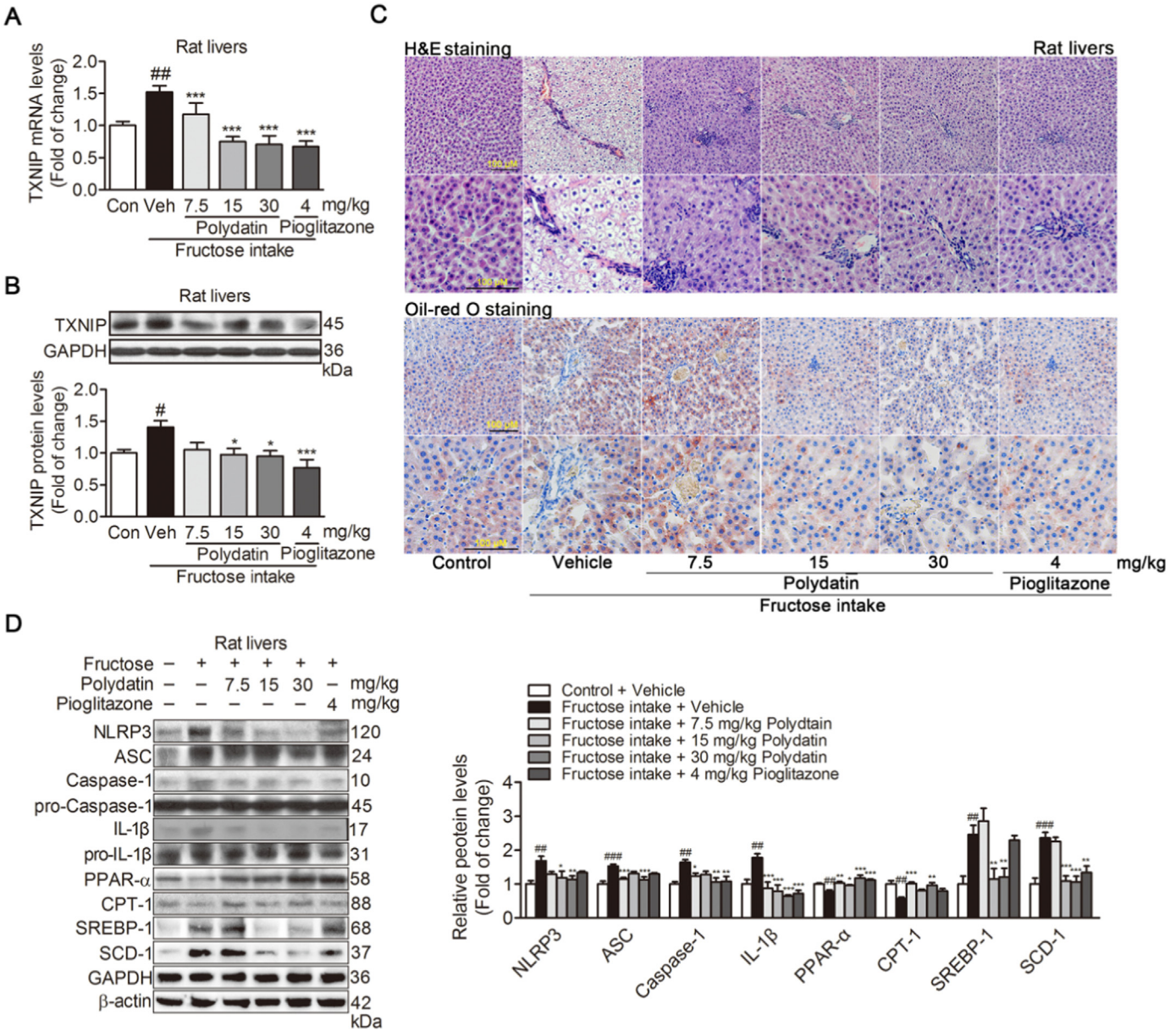

Fig. 1. Polydatin alleviates liver inflammation and lipid deposition in fructose-fed rats. Rats were fed 10% fructose drinking water (wt/vl) for 13 weeks and treated with polydtain (7.5, 15, 30 mg/kg) and pioglitazone (4 mg/kg) during the last 7 weeks. (A) qRT-PCT analysis of TXNIP mRNA levels, and (B) Western blot analysis of TXNIP protein levels in rat livers (n = 4 at least). Relative mRNA levels of TXNIP were normalized to β-actin. Relative protein levels of TXNIP were normalized to GAPDH. (C) Representative microphotograph of H&E-stained and oil-red O-stained paraffin-embedded sections of liver tissues were shown (200 and 400× magnification; bars, 100 μm), respectively. (D) Western blot analysis of NLRP3, ASC, Caspase-1, IL-1β, PPAR-α, CPT-1, SREBP-1 and SCD-1 protein levels in rat livers (n = 4 at least). Relative protein levels of Caspase-1 were normalized to pro-Caspase-1, of IL-1β were normalized to pro-IL-1β, of TXNIP, NLRP3, ASC, PPAR-α, CPT-1, SREBP-1 and SCD-1 were normalized to GAPDH or β-actin, respectively. All data are expressed as mean ± S.E.M.. *P* value was calculated by one-way ANOVA and further post hoc Dannelt testing. $^{\#}P < 0.05$, $^{\#\#}P < 0.01$, $^{\#\#\#}P < 0.001$ compared with control-vehicle; $^{*}P < 0.05$, $^{**}P < 0.01$, $^{***}P < 0.001$ compared with fructose-vehicle. TXNIP, thioredoxin-interacting protein; NLRP3, The NOD-like receptor (NLR) family, pyrin domain containing 3; ASC, apoptosis-associated speck-like protein; IL-1β, interleukin-1β; PPAR-α, peroxisome proliferator activated receptor-α; CPT-1, carnitine palmitoyl transferase-1; SREBP-1, sterol regulatory element binging protein 1; SCD-1, stearoyl-CoA desaturase-1.

3.2. Polydatin inhibits ROS/TXNIP to reduce inflammation and lipid deposition in fructose-exposed BRL-3A and HepG2 cells

In earlier study using HepG2 cells, we found that ROS-induced TXNIP drove fructose-mediated hepatic inflammation and lipid deposition through NLRP3 inflammasome activation [2]. In the present study, to address blockade of ROS-driven TXNIP to reduce inflammation and lipid deposition, first, we treated fructose-exposed BRL-3A cells with NAC in the presence of polydatin or pioglitazone for 48 h, and found that polydtain and pioglitazone significantly down-regulated TXNIP protein levels (Fig. 3A).

Next, we transfected BRL-3A cells with *TXNIP* siRNA (Supplementary Fig. 1A) for 24 h and then co-cultured with fructose, and polydatin or pioglitazone for 48 h, respectively. *TXNIP* siRNA failed to alter fructose-induced ROS levels in BRL-3A cells (Fig. 3B), further demonstrating that TXNIP over-expression was a downstream event in fructose-induced ROS production. Polydatin and pioglitazone significantly restrained fructose-induced ROS in *TXNIP* siRNA-transfected BRL-3A cells (24 h) (Fig. 3B). Consistently, they remarkably down-regulated protein levels of NLRP3, ASC and Caspase-1, reduced IL-1β

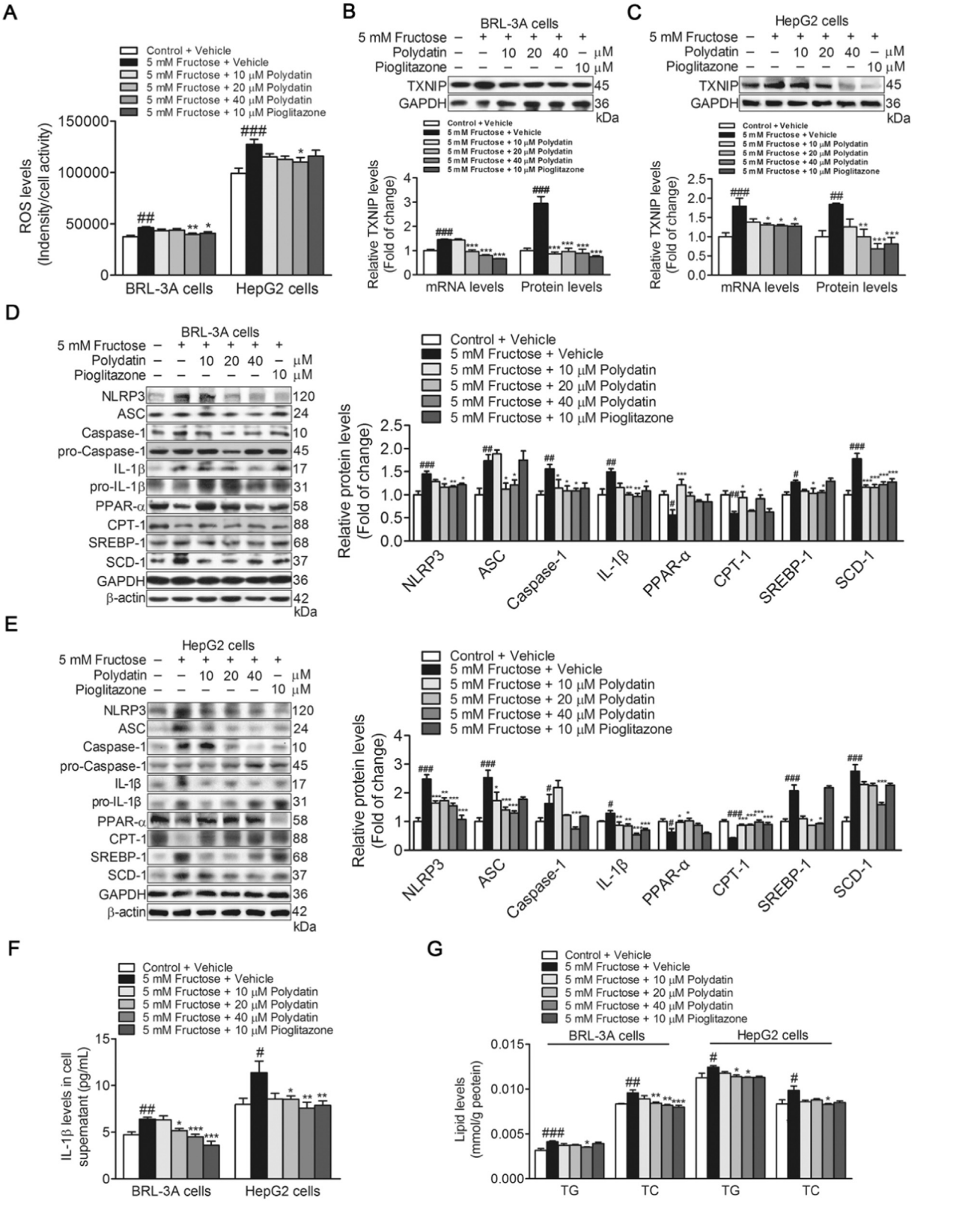

(caption on next page)

production, restored deregulation of PPAR-α, CPT-1, SREBP-1 and SCD-1 (Fig. 3C) with high TG and TC levels (Fig. 3D and E) in *TXNIP* siRNA-transfected BRL-3A cells with presence of fructose (48 h). These results suggest that blockade of fructose-induced oxidative stress by polydatin may be responsible for its attenuation of hepatic inflammation and lipid deposition.

Fig. 2. Polydatin reduces fructose-induced oxidative stress, inflammation and lipid accumulation in BRL-3A and HepG2 cells. BRL-3A and HepG2 cells were cultured with or without 5 mM fructose in the presence or absence of polydatin (10, 20 and 40 μM) or pioglitazone (10 μM), respectively. (A) ROS levels were analyzed by labeling fluorogenic probe $DCFH_2$-DA (n = 8). (B, C) qRT-PCT analysis of TXNIP mRNA levels and Western blot analysis of TXNIP protein levels in BRL-3A and HepG2 cells (48 h) (n = 4 at least). Relative mRNA levels of TXNIP were normalized to β-actin. Relative protein levels of TXNIP were normalized to GAPDH. (D, E) Western blot analysis of NLRP3, ASC, Caspase-1, IL-1β, PPAR-α, CPT-1, SREBP-1 and SCD-1 protein levels in BRL-3A and HepG2 cells (48 h) (n = 4 at least). Relative protein levels of Caspase-1 were normalized to pro-Caspase-1, of IL-1β were normalized to pro-IL-1β, of TXNIP, NLRP3, ASC, PPAR-α, CPT-1, SREBP-1 and SCD-1 were normalized to GAPDH or β-actin, respectively. (F) IL-1β levels were detected by ELISA in the supernatant of BRL-3A and HepG2 cells (24 h) (n = 4 at least). (G) TG and TC levels were measured with standard diagnostic kits in BRL-3A and HepG2 cells (48 h) (n = 4 at least). All data are expressed as mean ± S.E.M.. *P* value was calculated by one-way ANOVA and further post hoc Dannelt testing. $^{\#}P < 0.05$, $^{\#\#}P < 0.01$, $^{\#\#\#}P < 0.001$ compared with control-vehicle; $^{*}P < 0.05$, $^{**}P < 0.01$, $^{***}P < 0.001$ compared with fructose-vehicle. ROS, reactive oxygen species.

3.3. Polydatin inhibits Keap1 to activate Nrf2 antioxidant pathway in fructose-exposed BRL-3A and HepG2 cells with inflammation and lipid deposition

In subsequent studies, we explored the effect of polydatin on Keap1/Nrf2 pathway in fructose-induced inflammation and lipid deposition. We observed that fructose significantly decreased protein levels of nuclear but not total Nrf2 (Fig. 4A, B), as well as Nrf2-dependent antioxidant enzymes GST, HO-1 and NQO1 protein levels in fructose-exposed BRL-3A and HepG2 cells (Fig. 4C, D), showing that fructose blocked Nrf2 antioxidant pathway. Next, we investigated whether inhibition of Nrf2 antioxidant pathway hampered ROS elimination to induce TXNIP-mediated inflammation and lipid deposition under high fructose condition. The pretreatment (8 h) of 10 μM tBHQ remarkably increased nuclear Nrf2, GST, HO-1 and NQO1 protein levels (Fig. 4E), and decreased ROS levels (Fig. 4F) in fructose-exposed BRL-3A cells (24 h). tBHQ also down-regulated TXNIP protein levels in fructose-exposed BRL-3A cells (48 h) (Fig. 4G), but knockdown of *TXNIP* with siRNA was unable to reverse fructose-induced decrease of nuclear Nrf2 in BRL-3A cells (24 h) (Fig. 4H), suggesting that TXNIP over-expression may act as a downstream event in Nrf2 antioxidant pathway inactivation in response to fructose exposure. Whereas, tBHQ deceased NLRP3, ASC, Caspase-1, IL-1β, SREBP-1 and SCD-1 protein levels, increased PPAR-α and CPT-1 protein levels (Supplementary Fig. 2A), and reduced TG and TC levels (Supplementary Fig. 2B and C) in fructose-exposed BRL-3A cells (48 h).

Nrf2 is constantly targeted for proteasomal degradation by Keap1 under unstressed condition [28]. In fact, Keap1 mRNA and protein levels were markedly increased in fructose-exposed BRL-3A and HepG2 cells (24 h) (Fig. 5A, B). However, tBHQ pre-treatment failed to affect fructose-induced Keap1 over-expression in BRL-3A cells (24 h) (Fig. 5C), indicating that Keap1 over-expression was upstream of Nrf2 antioxidant pathway inactivation induced by fructose. Thus, to clarify the role of Keap1 on Nrf2 antioxidant pathway, we transfected BRL-3A cells with 50 nM *Keap1* siRNA for 24 h before fructose exposure (Supplementary Fig. 1B). *Keap1* siRNA significantly increased nuclear Nrf2, GST, NQO1 and HO-1 protein levels (Fig. 5D), and reduced ROS production (Fig. 5E) (24 h), as well as down-regulated TXNIP, NLRP3, ASC, Caspase-1, IL-1β, SREBP-1 and SCD-1, and up-regulated PPAR-α and CPT-1 (Supplementary Fig. 3A), with the reduction of TG and TC levels (Supplementary Fig. 3B and C) (48 h) in fructose-exposed BRL-3A cells. These observations indicate that Keap1 induction may block Nrf2 antioxidant pathway in fructose-induced inflammation and lipid deposition in BRL-3A cells.

As expected, polydatin and pioglitazone markedly increased protein levels of nuclear but not total Nrf2 (Fig. 4A, B), as well as GST, HO-1 and NQO1 (Fig. 4C, D) in fructose-exposed BRL-3A and HepG2 cells (24 h). In tBHQ pre-treated BRL-3A cells co-cultured with fructose, polydatin and pioglitazone up-regulated nuclear Nrf2, GST, HO-1 and NQO1 protein levels (Fig. 4E), reduced ROS levels (Fig. 4F) (24 h), and decreased TXNIP protein levels (Fig. 4G), consistently, inhibited NLRP3 inflammasome activation, IL-1β over-production, up-regulated PPAR-α and CPT-1 and down-regulated SREBP-1 and SCD-1 (Supplementary Fig. 2A) with TG and TC reduction (Supplementary Fig. 2B and C) (48 h). Of note, they significantly increased nuclear Nrf2 protein levels in *TXNIP* siRNA-transfected BRL-3A cells (24 h) (Fig. 4H).

Furthermore, polydatin and pioglitazone significantly decreased Keap1 mRNA and protein levels (Fig. 5A, B) in fructose-exposed BRL-3A and HepG2 cells (24 h). They remarkably decreased Keap1 protein levels (Fig. 5C) in tBHQ-pretreated BRL-3A co-cultured with fructose (24 h). Additionally, polydatin and pioglitazone remarkably up-regulated nuclear Nrf2, GST, HO-1 and NQO1 protein levels (Fig. 5D) with low ROS production (Fig. 5E) (24 h), down-regulated TXNIP, NLRP3, ASC, Caspase-1, IL-1β, SREBP-1 and SCD-1, up-regulated PPAR-α and CPT-1 (Supplementary Fig. 3A), and reduced TG and TC levels (Supplementary Fig. 3B and C) (48 h) in *Keap1* siRNA-transfected BRL-3A cells exposed to fructose. These data prove that polydatin and pioglitazone inhibit Keap1 to activate Nrf2 antioxidant pathway in the reduction of fructose-induced inflammation and lipid deposition in BRL-3A cells.

3.4. Polydatin enhances miR-200a expression targeting Keap1 to activate Nrf2 antioxidant pathway in fructose-exposed BRL-3A and HepG2 cells with inflammation and lipid deposition

To further elucidate the mechanisms controlling Keap1/Nrf2 pathway in fructose-induced hepatic inflammation and lipid deposition, we detected miR-200a expression in response to fructose in cell cultures. Here, we noted that miR-200a expression profiling was significantly decreased in fructose-exposed BRL-3A (4 h) and HepG2 cells (12 h) (Fig. 6A), which were consistent with fructose-induced increase in Keap1 (Fig. 5A, B). Interestingly, *TargetScan 5.2.* predicted that Keap1 was as one of miR-200a target genes. To examine this prediction, the wild type 3′-UTR or the mutant 3′-UTR target sequence (Fig. 6B) were cloned into the luciferase reporter vector. These vectors were transfected into BRL-3A and HepG2 cells with miR-200a mimic, and found that miR-200a mimic significantly decreased wild type Keap1 3′-UTR reporter activity, but failed to alter mutant Keap1 3′-UTR reporter activity (Fig. 6B), the negative control affected neither wild type nor mutant Keap1 3′-UTR reporter activity (Fig. 6B). Additionally, *Keap1* siRNA transfection was unable to alter miR-200a expression (4 h) (Fig. 6C) in BRL-3A co-cultured with fructose. These results provide the evidence that miR-200a may target the predicted site within the 3′-UTR of Keap1 mRNA.

In the following experiments, we assessed the role of miR-200a targeting Keap1/Nrf2 pathway on oxidative stress-enhanced inflammation and lipid deposition. We successfully transfected BRL-3A cells with 50 nM miR-200a mimic (Supplementary Fig. 1C). MiR-200a mimic transfection significantly down-regulated Keap1 protein levels, then up-regulated Nrf2 nuclear, GST, HO-1 and NQO1 protein levels (Fig. 6D), abrogated over-production of ROS (Fig. 6E) (24 h), reversed over-expression of TXNIP, up-regulation of NLRP3, ASC, Caspase-1 and IL-1β, deregulation of PPAR-α, CPT-1, SREBP-1 and SCD-1 (Supplementary Fig. 4A), with TG and TC deposition (Supplementary Fig. 4B and C) (48 h) in BRL-3A cells exposed to fructose. These results indicate that fructose may decrease miR-200a expression to up-regulate Keap1, and subsequently block Nrf2 antioxidant pathway to cause oxidative stress, inflammation and lipid deposition in BRL-3A cells.

We observed that polydatin markedly increased miR-200a expression in BRL-3A (4 h) and HepG2 (12 h) cells under high fructose

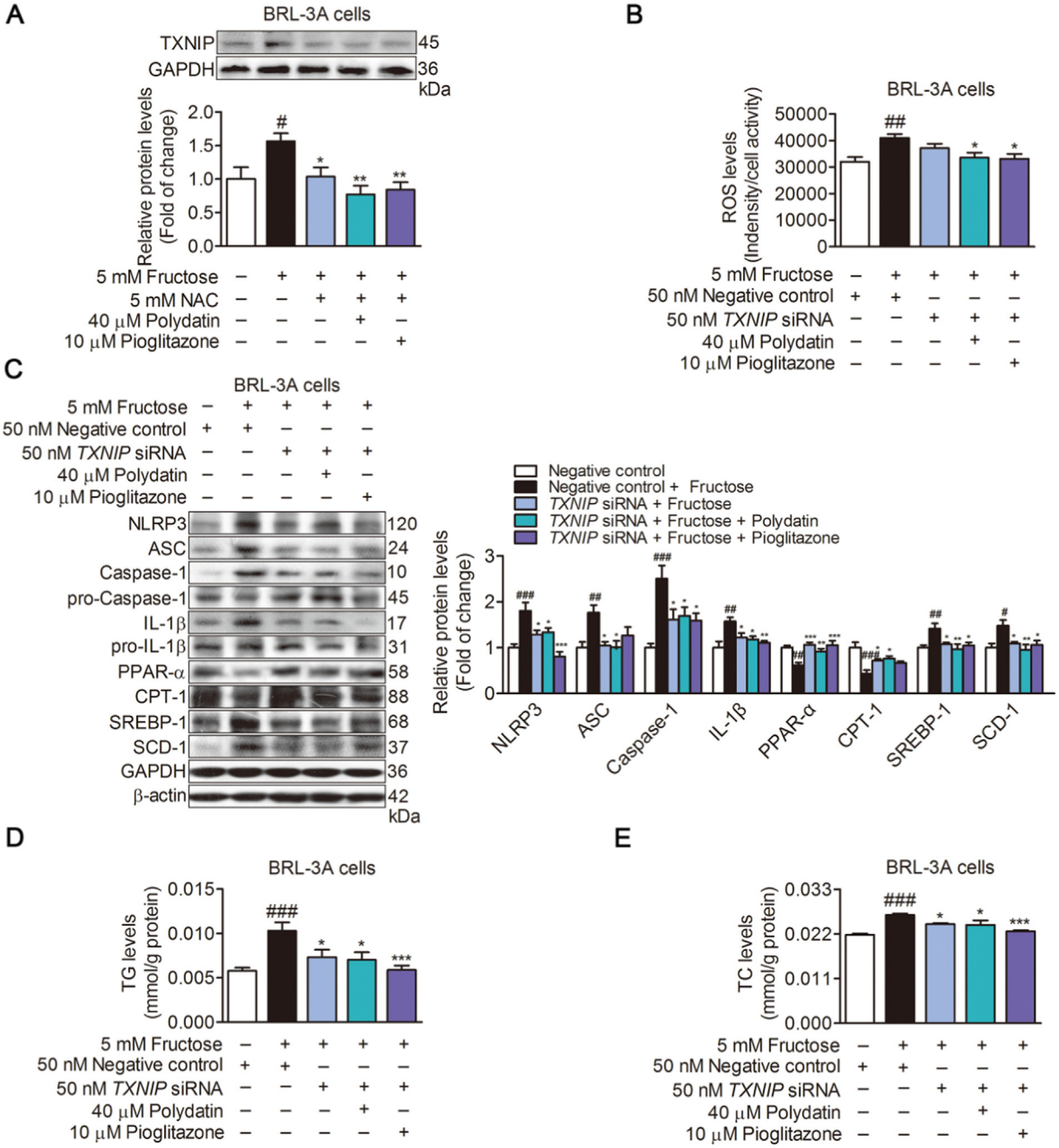

Fig. 3. Polydatin inhibits ROS/TXNIP to reduce inflammation and lipid deposition in fructose-exposed BRL-3A cells. (A) Western blot analysis of TXNIP protein levels in 5 mM NAC treated BRL-3A cells incubated with 5 mM fructose in the presence or absence of 40 μM polydatin or 10 μM pioglitazone (48 h) (n = 4 at least). Relative protein levels of TXNIP were normalized to GAPDH. (B) Assay of ROS levels (24 h, n = 7 at least), (C) Western blot analysis of NLRP3, ASC, Caspase-1, IL-1β, PPAR-α, CPT-1, SREBP-1 and SCD-1 protein levels (48 h) (n = 4 at least), and detection of TG (D) and TC (E) levels (48 h) (n = 4 at least) in *TXNIP* siRNA-transfected BRL-3A cells incubated with 5 mM fructose in the presence or absence of 40 μM polydatin or 10 μM pioglitazone. Relative protein levels of Caspase-1 were normalized to pro-Caspase-1, of IL-1β were normalized to pro-IL-1β, of TXNIP, NLRP3, ASC, PPAR-α, CPT-1, SREBP-1 and SCD-1 were normalized to GAPDH or β-actin, respectively. All data are expressed as mean ± S.E.M.. *P* value was calculated by one-way ANOVA and further post hoc Dannelt testing. $^{\#}P < 0.05$, $^{\#\#}P < 0.01$, $^{\#\#\#}P < 0.001$ compared with control-vehicle; $^{*}P < 0.05$, $^{**}P < 0.01$, $^{***}P < 0.001$ compared with fructose-vehicle. NAC, *N*-acetyl-L-cysteine.

induction (Fig. 6A). It significantly increased miR-200a expression in *Keap1* siRNA-transfected BRL-3A cells co-cultured with fructose (24 h) (Fig. 6C). Polydatin also succeeded in down-regulation of Keap1 protein levels, up-regulation of Nrf2 nuclear, GST, HO-1 and NQO1 protein levels (Fig. 6D), decrease of ROS production (Fig. 6E) (24 h), as well as decrease of TXNIP, NLRP3, ASC, Caspase-1 and IL-1β protein levels, restoration of PPAR-α, CPT-1, SREBP-1 and SCD-1 change (Supplementary Fig. 4A), with reduction of TG and TC levels (Supplementary Fig. 4B and C) (48 h) in miR-200a mimic-transfected BRL-3A cells exposed to fructose. Pioglitazone also exhibited the similar effects in these cell models (Fig. 5). Our findings indicate that polydatin and pioglitazone may increase miR-200a expression targeting Keap1 to activate Nrf2 antioxidant pathway in the attenuation of fructose-induced oxidative stress, inflammation and lipid deposition in BRL-3A cells.

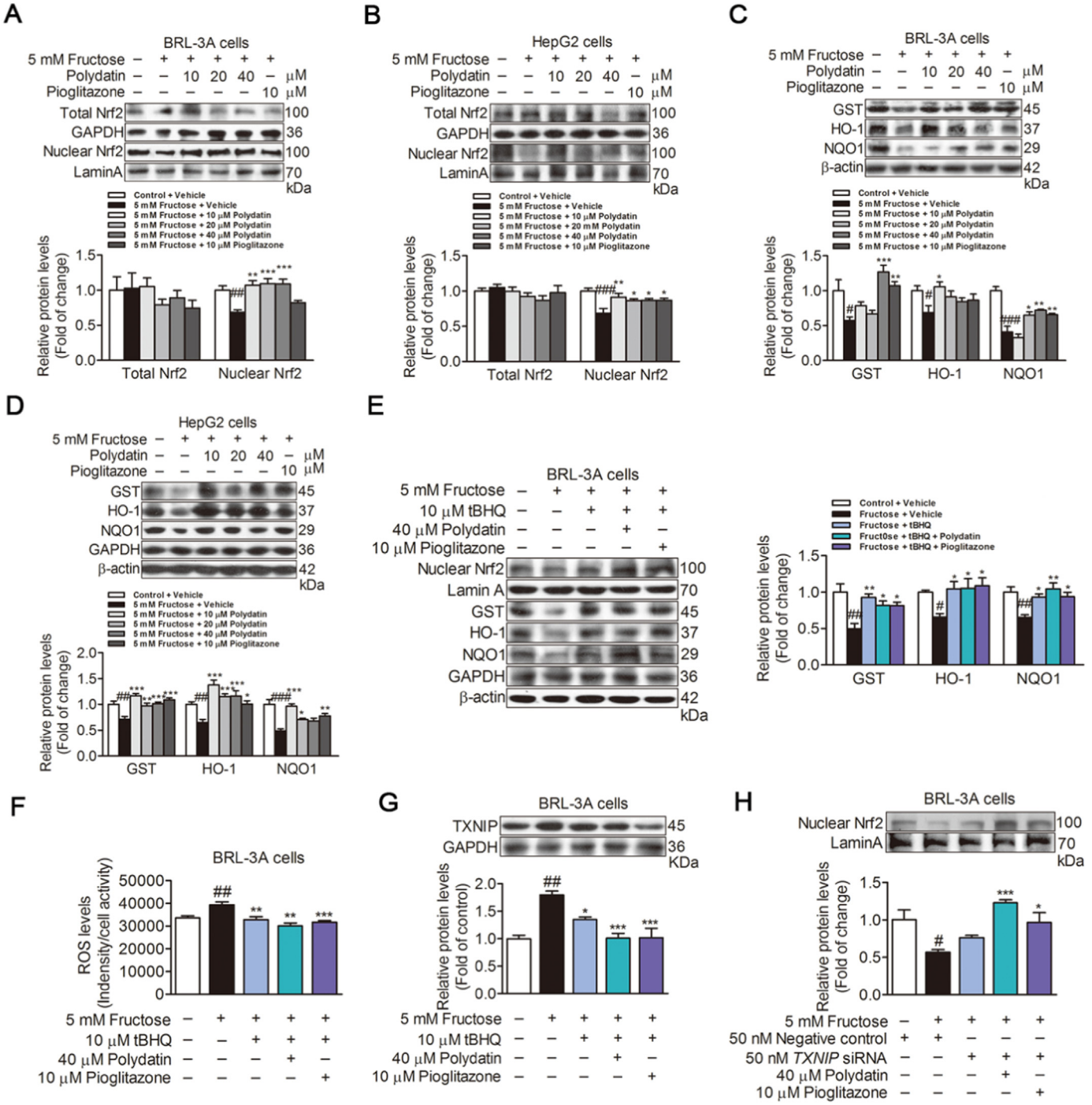

Fig. 4. Polydatin activates Nrf2 antioxidant pathway to inhibit oxidative stress in fructose-exposed BRL-3A and HepG2 cells. (A, B) Western blot analysis of total and nuclear Nrf2 protein levels in BRL-3A and HepG2 cells (24 h) (n = 4 at least). (C, D) Western blot analysis of GST, HO-1 and NQO1 protein levels in BRL-3A and HepG2 cells (24 h) (n = 4 at least). (E) Western blot analysis of nuclear Nrf2, GST, HO-1 and NQO1 protein levels (24 h) (n = 4 at least), (F) assay of ROS levels (24 h) (n = 5 at laest), (G) Western blot analysis of TXNIP protein levels (48 h) (n = 4 at least) in 10 μM tBHQ pretreated-BRL-3A cells for 8 h incubated with 5 mM fructose in the presence or absence of 40 μM polydatin or 10 μM pioglitazone, respectively. (H) Western blot analysis of nuclear Nrf2 protein levels in *TXNIP* siRNA-transfected BRL-3A cells incubated with 5 mM fructose in the presence or absence of 40 μM polydatin or 10 μM pioglitazone (24 h) (n = 4 at least). Relative protein levels of nuclear Nrf2 were normalized to LaminA, of total Nrf2, GST, HO-1 and NQO1 were normalized to GAPDH or β-actin, respectively. All data are expressed as mean ± S.E.M.. *P* value was calculated by one-way ANOVA and further post hoc Dannelt testing. $^{\#}P < 0.05$, $^{\#\#}P < 0.01$, $^{\#\#\#}P < 0.001$ compared with control-vehicle; $^{*}P < 0.05$, $^{**}P < 0.01$, $^{***}P < 0.001$ compared with fructose-vehicle. Nrf2, nuclear factor erythroid 2-related factor 2; GST, glutathione S-transferase; HO-1, hemeoxygenase-1; NQO1, NAD(P)H: quinone oxidoreductase 1.

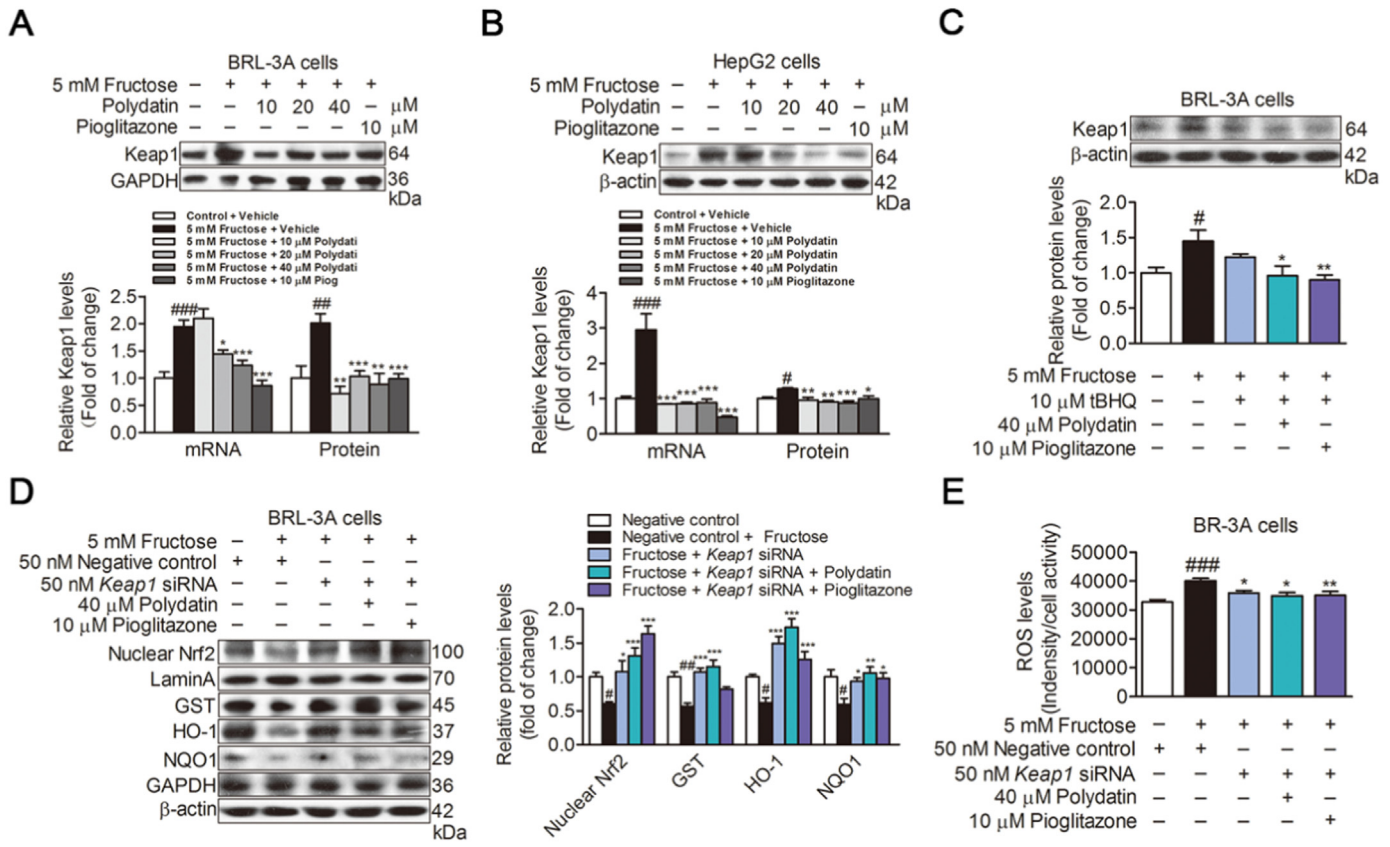

Fig. 5. Polydatin inhibits Keap1 to activate Nrf2 antioxidant pathway and inhibit oxidative stress in fructose-exposed BRL-3A and HepG2 cells. (A, B) qRT-PCT analysis of Keap1 mRNA levels and Western blot analysis of Keap1 protein levels in BRL-3A and HepG2 cells (24 h) (n = 4 at least). Relative mRNA levels of Keap1 were normalized to β-actin. (C) Western blot analysis of Keap1 protein levels (24 h) (n = 4 at least) in 10 μM tBHQ pretreated-BRL-3A cells for 8 h incubated with 5 mM fructose in the presence or absence of 40 μM polydatin or 10 μM pioglitazone. (D) Western blot analysis of nuclear Nrf2, GST, HO-1 and NQO1 protein levels (24 h) (n = 4 at least), (E) assay of ROS levels (24 h) (n = 6 at least) in 50 nM *Keap1* siRNA transfected-BRL-3A cells incubated with 5 mM fructose in the presence or absence of 40 μM polydatin or 10 μM pioglitazone, respectively. Relative protein levels of nuclear Nrf2 were normalized to LaminA, of Keap1, total Nrf2, GST, HO-1 and NQO1 were normalized to GAPDH or β-actin, respectively. All data are expressed as mean ± S.E.M.. *P* value was calculated by one-way ANOVA and further post hoc Dannelt testing. $^{\#}P < 0.05$, $^{\#\#}P < 0.01$, $^{\#\#\#}P < 0.001$ compared with control-vehicle; $^{*}P < 0.05$, $^{**}P < 0.01$, $^{***}P < 0.001$ compared with fructose-vehicle. Keap1, Kelch-like ECH-associated protein 1.

3.5. Polydatin attenuates fructose feeding-induced miR-200a low-expression, Keap1 up-regulation and Nrf2 antioxidant pathway inactivation in rats

To get an estimate of the potential relevance of these findings, we detected miR-200a expression and Keap1/Nrf2 pathway in the liver of fructose-fed rats with oxidative stress, inflammation and lipid disposition. Interestingly, we noticed a low-expression of liver miR-200a (Fig. 7A) in fructose-fed rats. We also observed fructose feeding up-regulated Keap1 mRNA and protein levels (Fig. 7B), as well as down-regulated nuclear Nrf2 (Fig. 7C), GST, HO-1 and NQO1 protein levels (Fig. 7D) in the liver of rats. Subsequently, we found that polydatin and pioglitazone increased miR-200a expression, down-regulated Keap1 and activated Nrf2 antioxidant pathway in this animal model (Fig. 7). A schematic model summarizing the mechanisms elucidated by our study was provided in Fig. 8.

4. Discussion

Non-alcoholic fatty liver disease is a common pathological manifestation of liver diseases and is known to aggravate the development of cirrhosis and hepatocellular carcinoma [1,29]. Fructose is present in industrialized foods and beverages in large amounts throughout the world. Clinical and experimental evidences demonstrate that excessive fructose consumption causes nonalcoholic fatty liver disease pathogenesis [1,2]. The enhanced oxidative stress signaling may underlie these events. Although clinical treatment with *P. cuspidatum* is available for the therapy of patients with many progressive liver diseases in Chinese medicine, the knowledge about the action of its main constituent polydatin is still fragmentary. Using an in vivo model induced by high fructose feeding, we provided evidence here that polydatin prevented miR-200a low-expression, Keap1 up-regulation and Nrf2 antioxidant pathway inactivation, being consistent with its reduction of liver inflammation and lipid deposition. Similar findings were obtained from in vitro studies using BRL-3A and HepG2 cells. These results provide new insight into the molecular factors that mediate the action of polydatin on fructose-induced oxidative stress, inflammation and lipid deposition and suggest new strategy for therapy.

Our previous study showed that ROS-driven TXNIP in fructose-induced liver inflammation and lipid deposition [2]. TXNIP binds to NLRP3 in response to ROS, causing NLRP3 inflammasome activation [8]. In this study, we also showed that TXNIP over-expression was a downstream event in ROS production in BRL-3A cells under high fructose stimulation. Of note, *TXNIP* siRNA only decreased one-third of TXNIP protein levels in fructose-exposed BRL-3A cells, possibly indicating that ROS-driven TXNIP and NLRP3 inflammasome activation was not completely interrupted. Thus, knockdown of TXNIP inhibited NLRP3 inflammasome activation and partly restored lipid metabolism-related protein abnormal expression, resulting in reduction of TG and

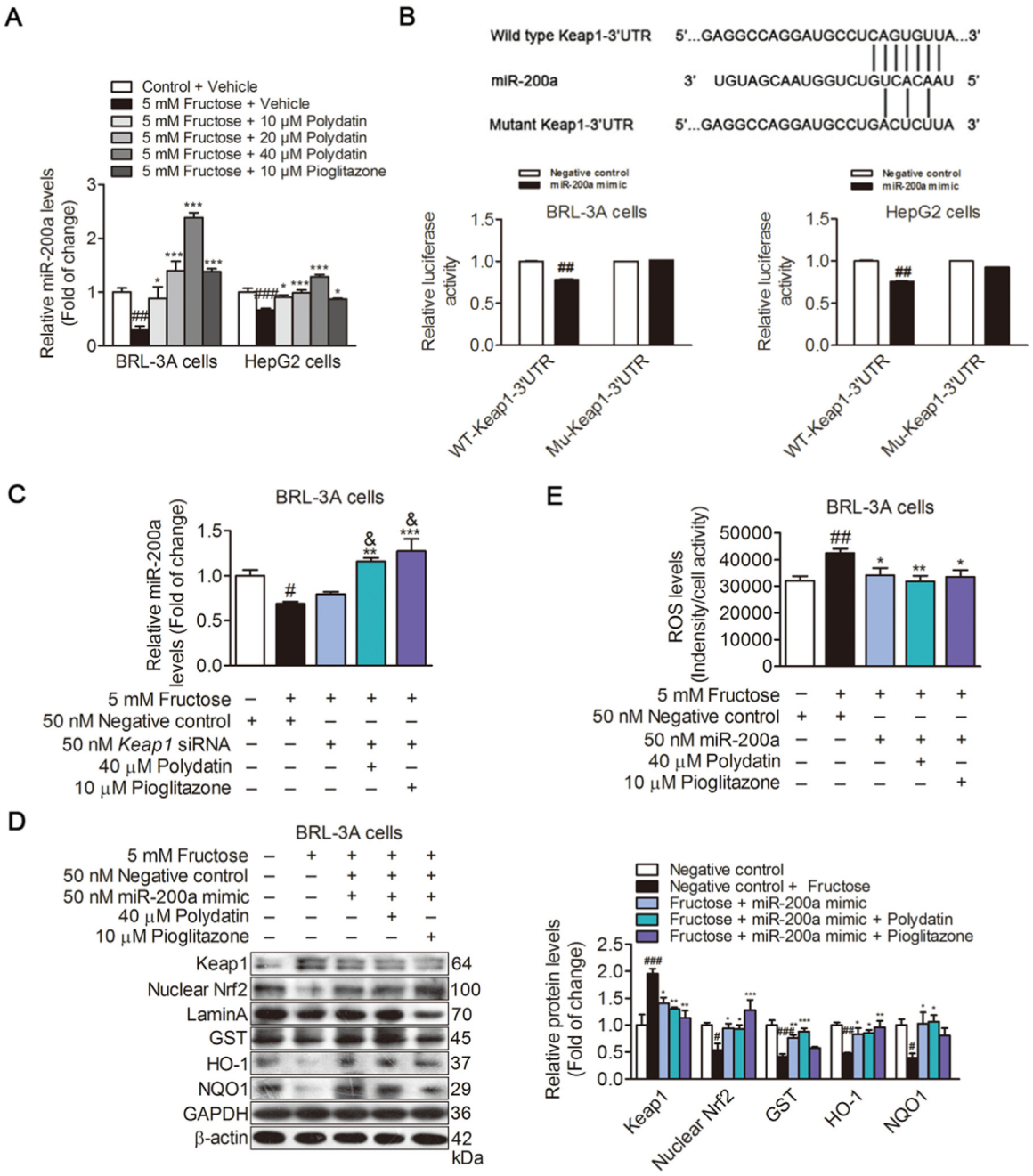

Fig. 6. Polydatin enhances miR-200a expression targeting Keap1 to activate Nrf2 antioxidant pathway in suppression of oxidative stress in fructose-exposed BRL-3A and HepG2 cells. (A) qRT-PCR analysis of miR-200a expression levels in BRL-3A (4 h) and HepG2 cells (12 h) (n = 4 at least). (B) Diagrams showed the miR-200a putative binding sites and corresponding mutant sites of Keap1. Dual-luciferase reporter assay of miR-200a with 3′UTR vectors (wild type or mutant) of rat keap1 in BRL-3A and HepG2 cells (n = 4 at least). (C) qRT-PCR analysis of miR-200a expression in 50 nM *Keap1* siRNA transfected-BRL-3A cells incubated with 5 mM fructose in the presence or absence of 40 μM polydatin or 10 μM pioglitazone (4 h) (n = 4 at least). (D) Western blot analysis of Keap1, nuclear Nrf2, GST, HO-1 and NQO1 protein levels (24 h) (n = 4 at least), (E) assay of ROS levels (24 h) (n = 8) in 50 nM miR-200a mimic transfected-BRL-3A cells incubated with 5 mM fructose in the presence or absence of 40 μM polydatin or 10 μM pioglitazone, respectively. Relative miR-200a levels were normalized to U6. Relative protein levels of nuclear Nrf2 were normalized to LaminA, of Keap1, total Nrf2, GST, HO-1 and NQO1 were normalized to GAPDH or β-actin, respectively. All data are expressed as mean ± S.E.M.. *P* value was calculated by one-way ANOVA and further post hoc Dannelt testing. $^{\#}P < 0.05$, $^{\#\#}P < 0.01$, $^{\#\#\#}P < 0.001$ compared with control-vehicle; $^{*}P < 0.05$, $^{**}P < 0.01$, $^{***}P < 0.001$ compared with fructose-vehicle; $^{\&}P < 0.05$ compared with fructose-*Keap1* siRNA. UTR, untranslated region.

TC levels in fructose-exposed BRL-3A cells.

Interestingly, Nrf2 antioxidant pathway is an essential cellular system to protect tissues from oxidative stress [30]. Specific Keap1 knockout prevents ethanol-induced ROS production, but Nrf2 deficiency aggravates ROS accumulation in mouse primary hepatocytes [11]. Nrf2 knockout induces heart TXNIP over-expression in diabetic mice [32]. This study found up-regulation of Keap1, down-regulation of Nrf2 nuclear translocation and its target antioxidant GST, HO-1 and NQO1, as well as high levels of ROS and TXNIP in fructose-fed rat livers and fructose-exposed BRL-3A and HepG2 cells. Moreover, we illuminated the relationship between Keap1 over-expression and Nrf2 antioxidant pathway inactivation induced by fructose. Nrf2 inhibition induced by fructose was mostly reversed by *Keap1* siRNA, whereas Nrf2 activator tBHQ pre-treatment failed to alter Keap1 in BRL-3A cells, indicating that Keap1 over-expression may act upstream of Nrf2 inactivation. Additionally, *Keap1* silence or Nrf2 activator tBHQ

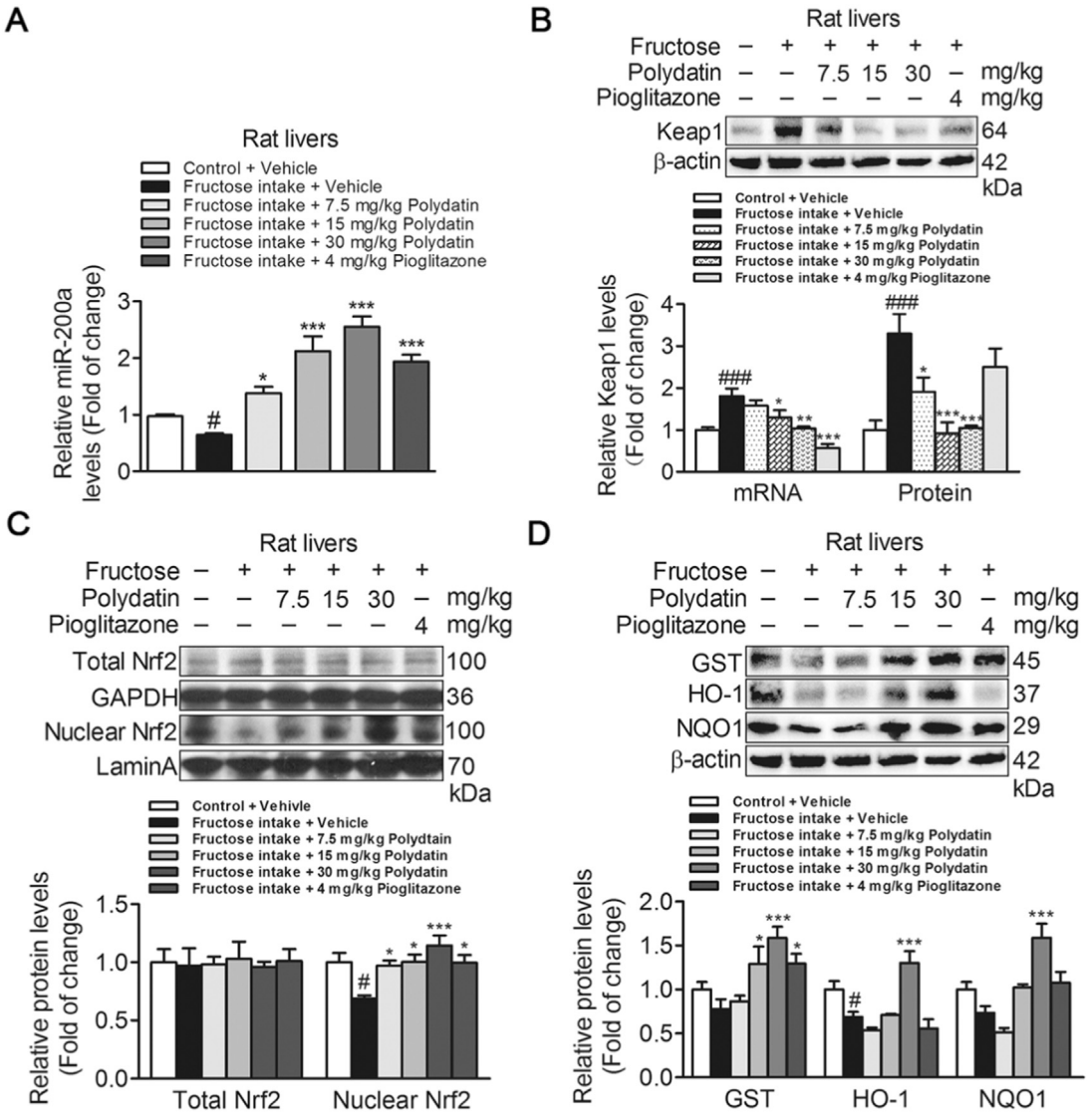

Fig. 7. Polydatin attenuates fructose feeding-induced miR-200a low-expression, Keap1 up-regulation and Nrf2 antioxidant pathway inactivation in rats with liver oxidative stress. (A) qRT-PCR analysis of miR-200a expression levels in rat livers. Relative miR-200a levels were normalized to U6. (B) qRT-PCT analysis of Keap1 mRNA levels and Western blot analysis of Keap1 protein levels in rat livers. Relative mRNA levels of Keap1 were normalized to β-actin. Western blot analysis of total Nrf2 and nuclear Nrf2 (C), GST, HO-1 and NQO1 protein levels (D) in rat livers. Relative protein levels of nuclear Nrf2 were normalized to LaminA, of Keap1, total Nrf2, GST, HO-1 and NQO1 were normalized to GAPDH or β-actin, respectively. All data are expressed as mean ± S.E.M. (n = 4 at least). *P* value was calculated by one-way ANOVA and further post hoc Dannelt testing. $^{\#}P < 0.05$, $^{\#\#}P < 0.01$, $^{\#\#\#}P < 0.001$ compared with control-vehicle; $^{*}P < 0.05$, $^{**}P < 0.01$, $^{***}P < 0.001$ compared with fructose-vehicle.

pretreatment promoted Nrf2 nuclear translocation and induction of GST, HO-1 and NQO1 to quench fructose-induced ROS and reversed TXNIP over-expression in BRL-3A cells. There observations indicate that fructose-induced oxidative stress may be at least partly due to Keap1-mediated inactivation of Nrf2 in BRL-3A cells.

tBHQ is reported to inhibit NLRP3 inflammasome activation and consequent IL-1β production and secretion in cerebral ischemia reperfusion injury of rats [33]. Keap1 knockout with maximum Nrf2 activation ameliorates ethanol-induced liver lipid deposition by up-regulating SREBP-1 and SCD-1 in mice [11]. Nrf2 knockdown inhibits PPAR-α and CPT-1 but enhances SREBP-1c to increase lipid droplets as well as TG and TC levels in ethanol-simulated human hepatocytes cell lines, however, Nrf2 over-expression plasmid reverses these changes [34]. In this study, siRNA-mediated Keap1 knockdown down-regulated TXNIP to suppress NLRP3 inflammation activation, resulting in the regulation of PPAR-α, CPT-1, REBP-1 and SCD-1 with the reduction of TG and TC levels in fructose-exposed BRL-3A cells. Although Nrf2 antioxidant pathway activation mediated by tBHQ pre-treatment was unable to change fructose-induced Keap1 over-expression, this event could rapidly quench ROS to block TXNIP and NLRP3 inflammasome activation, and then restore lipid metabolism relative protein abnormal expression as well as TG and TC content reduction in BRL-3A cells. These results demonstrate that fructose-induced inhibition of Nrf2 antioxidant pathway via Keap1 may develop liver inflammation and lipid deposition.

Recently, more studies focus on the regulatory effects of miRNAs on redox homeostasis [31,35,36] MiR-200a is low-expression in hypoxia-exposed human adult cardiomyocyte line with oxidative stress [12]. However, little attention has been paid to miR-200a in fructose-induced liver oxidative stress, inflammation and lipid deposition. Interestingly, we found that Keap1 was a target gene of miR-200a in BRL-3A and HepG2 cells, and miR-200a low-expression was consistent with Keap1 up-regulation in fructose-fed rat livers and fructose-exposed BRL-3A and HepG2 cells. Moreover, miR-200a high-expression nearly

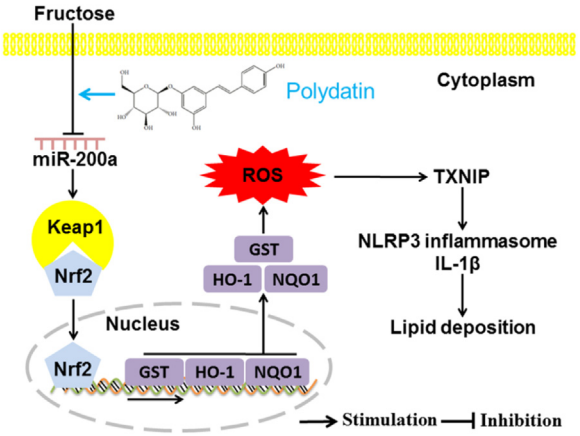

Fig. 8. The hypothetical mechanisms by which polydatin prevents fructose-induced in liver inflammation and lipid deposition through increasing miR-200a to regulate Keap1/Nrf2 pathway. Fructose-induced miR-200a low-expression increased Keap1 to inhibit Nrf2 antioxidant pathway, and then caused ROS-driven TXNIP to promote NLRP3 inflammasome activation and lipid metabolism-related protein dysregulation, resulting in liver inflammation and lipid deposition. Polydatin protected fructose-induced liver inflammation and lipid deposition by which increased miR-200a expression to decrease Keap1 and activate Nrf2 antioxidant pathway, and then blocked ROS-driven TXNIP to suppress NLRP3 inflammasome activation and regulated lipid metabolism-related proteins.

abrogated fructose-induced keap1 up-regulation and Nrf2 antioxidant pathway inactivation, and then ROS over-production and TXNIP over-expression in BRL-3A cells. Of note, aberrant miR-200a expression triggers TNF-α expression and inhibits PPAR-α, as well as increases SREBP-1c and SCD1 in fructose-exposed HepG2 cells [13]. Indeed, this study found that miR-200a mimic transfection reversed fructose-induced TXNIP-driven NLRP3 inflammasome activation, IL-1β production, and deregulation of PPAR-α, CPT-1, SREBP-1 and SCD-1 as well as TG and TC deposition in BRL-3A cells. Collectively, these results support the evidence that Keap1/Nrf2 pathway mediated by miR-200a low-expression is a key regulator of oxidative stress in fructose-induced liver inflammation and lipid deposition. This could be of potential therapeutic relevance.

In earlier reports, polydatin suppresses NLRP3 inflammasome activation and ameliorates potassium oxonate-induced kidney inflammation in rats [20], and enhances PPAR-α and inhibits SCD-1 in animal models induced by streptozocin or a high-fat diet [21,22]. In this study, we observed that polydatin and pioglitazone restored fructose-induced TXNIP over-expression, NLRP3 inflammasome activation, IL-1β production and secretion, and deregulation of PPAR-α, CPT-1, SREBP-1 and SCD-1 with TG and TC deposition in rat livers and BRL-3A and HepG2 cells. Enhancement of Nrf2 nuclear translocation through Keap1 silence up-regulates HO-1 and inhibits palmitate-induced ROS over-production in HepG2 cells [6]. We also found that polydatin and pioglitazone decreased Keap1 mRNA and protein levels, increased Nrf2 nuclear translocation with induction of GST, HO-1 and NQO1 to reduce ROS production in fructose-fed rats and fructose-exposed BRL-3A and HepG2 cells. Further results from *Keap1* siRNA and tBHQ pretreatment supported that polydatin and pioglitazone effectively down-regulated Keap1 to activate Nrf2 antioxidant pathway, resulting in the suppression of ROS-driven TXNIP and NLRP3 inflammasome activation as well as normalization of lipid metabolism-related proteins in BRL-3A cells.

MiR-200a high-expression can inhibit Keap1 and activate Nrf2 antioxidant pathway, and then quench ROS [12]. In this study, we firstly found that polydatin and pioglitazone up-regulated miR-200a expression in rat livers and BRL-3A and HepG2 cells under high fructose stimulation. Moreover, they up-regulated miR-200a to down-regulate Keap1 and activate Nrf2 antioxidant pathway to repress ROS-driven TXNIP and NLRP3 inflammasome activation as well as lipid metabolism-related protein dysregulation. Therefore, the regulation of polydatin and pioglitazone on miR-200a-targeted Keap1/Nrf2 pathway is required for the attenuation of fructose-induced inflammation and lipid deposition in BRL-3A cells. Taken together, these data further support the evidence that polydatin and pioglitazone reduce oxidative stress by increasing miR-200a to regulate Keap1/Nrf2 pathway in the protection against fructose-induced liver inflammation and lipid deposition.

In conclusion, our data for the first time demonstrated that fructose-induced miR-200a low-expression increased Keap1 to inhibit Nrf2 antioxidant pathway, and then caused ROS-driven TXNIP to promote NLRP3 inflammasome activation and lipid metabolism-related protein dysregulation, resulting in liver inflammation and lipid deposition. Polydatin increased miR-200a expression to decrease Keap1 and activate Nrf2 antioxidant pathway, and then blocked ROS-driven TXNIP to suppress NLRP3 inflammasome activation and regulated lipid metabolism-related proteins, protecting against fructose-induced inflammation and lipid deposition. This study supports the notion that the enhancement of miR-200a to control Keap1/Nrf2 pathway by hepatoprotection agent polydatin is a therapeutic strategy for the prevention and treatment of fructose-associated liver inflammation and lipid deposition.

Acknowledgment

This work was supported by Grant from National Natural Science Foundation of China (No. 81573667 and 81730105) to Ling-Dong Kong.

Competing interests

The authors declare no competing financial interests.

Authors' contributions

Ling-Dong Kong designed the experiments. Xiao-Juan Zhao carried out animal and cell experiments; Yang-Zi Yang, Tian-Yu Chen, Lin-Lin Kang and Ke-Ke Jia helped animal experiments; Han-Wen Yu and Rui-Qing Jiao helped cell culture, immunohistochemistry and immunofluorescence experiments; Wen-Yuan Wu helped dual luciferase reporter assay; Xiao-Juan Zhao and Ling-Dong Kong analyzed data; Ling-Dong Kong and Xiao-Juan Zhao wrote the manuscript.

Appendix A. Supporting information

Supplementary data associated with this article can be found in the online version at doi:10.1016/j.redox.2018.07.002.

References

[1] M.B. Vos, J.E. Lavine, Dietary fructose in nonalcoholic fatty liver disease, Hepatology 57 (2013) 2525–2531.
[2] X. Zhang, J.H. Zhang, X.Y. Chen, Q.H. Hu, M.X. Wang, R. Jin, Q.Y. Zhang, W. Wang, R. Wang, L.L. Kang, J.S. Li, M. Li, Y. Pan, J.J. Huang, L.D. Kong, Reactive oxygen species-induced TXNIP drives fructose-mediated hepatic inflammation and lipid accumulation through NLRP3 inflammasome activation, Antioxid. Redox Signal. 22 (2015) 848–870.
[3] S. Spahis, E. Delvin, J.M. Borys, E. Levy, Oxidative stress as a critical factor in nonalcoholic fatty liver disease pathogenesis, Antioxid. Redox Signal. 26 (2017) 519–541.
[4] R. Sabouny, E. Fraunberger, M. Geoffrion, A.C. Ng, S.D. Baird, R.A. Screaton, R. Milne, H.M. McBride, T.E. Shutt, The Keap1-Nrf2 stress response pathway promotes mitochondrial hyperfusion through degradation of the mitochondrial fission protein Drp1, Antioxid. Redox Signal. 27 (2017) 1447–1459.
[5] Y. Zhao, W. Song, Z. Wang, Z. Wang, X. Jin, J. Xu, L. Bai, Y. Li, J. Cui, L. Cai, Resveratrol attenuates testicular apoptosis in type 1 diabetic mice: role of Akt-mediated Nrf2 activation and p62-dependent Keap1 degradation, Redox Biol. 14 (2018) 609–617.
[6] C.H. Yan, W.Y. Sun, X. Wang, J.G. Long, X.B. Liu, Z.H. Feng, J.K. Liu, Punicalagin attenuates palmitate-induced lipotoxicity in HepG2 cells by activating the Keap1-Nrf2 antioxidant defense system, Mol. Nutr. Food Res. 60 (2016) 1139–1149.
[7] H. Lv, Q. Liu, Z. Wen, H. Feng, X. Deng, X. Ci, Xanthohumol ameliorates

lipopolysaccharide (LPS)-induced acute lung injury via induction of AMPK/GSK3beta-Nrf2 signal axis, Redox Biol. 12 (2017) 311–324.
[8] R. Zhou, A. Tardivel, B. Thorens, I. Choi, J. Tschopp, Thioredoxin-interacting protein links oxidative stress to inflammasome activation, Nat. Immunol. 11 (2010) 136–140.
[9] X. Liu, X. Zhang, Y. Ding, W. Zhou, L. Tao, P. Lu, Y. Wang, R. Hu, Nuclear factor E2-related factor-2 negatively regulates NLRP3 inflammasome activity by inhibiting reactive oxygen species-induced NLRP3 priming, Antioxid. Redox Signal. 26 (2017) 28–43.
[10] N. Keleku-Lukwete, M. Suzuki, M. Yamamoto, An overview of the advantages of KEAP1-NRF2 system activation during inflammatory disease treatment, Antioxid. Redox Signal. (2017) Epub.
[11] K.C. Wu, J. Liu, C.D. Klaassen, Role of Nrf2 in preventing ethanol-induced oxidative stress and lipid accumulation, Toxicol. Appl. Pharmacol. 252 (2012) 321–329.
[12] X. Sun, H. Zuo, C. Liu, Y. Yang, Overexpression of miR-200a protects cardiomyocytes against hypoxia-induced apoptosis by modulating the kelch-like ECH-associated protein 1-nuclear factor erythroid 2-related factor 2 signaling axis, Int. J. Mol. Med. 38 (2016) 1303–1311.
[13] P. Zhang, L. Xu, H. Guan, L. Liu, J. Liu, Z. Huang, X. Cao, Z. Liao, H. Xiao, Y. Li, Beraprost sodium, a prostacyclin analogue, reduces fructose-induced hepatocellular steatosis in mice and in vitro via the microRNA-200a and SIRT1 signaling pathway, Metabolism 73 (2017) 9–21.
[14] Q.H. Zhou, Polygonum cuspidatum clinical application and overview of experimental research, Shanxi J. Tradit. Chin. Med. 6 (1985) 42–43.
[15] Q.L. Jiang, J. Ma, J.Y. Pan, Y.Y. Li, J.Y. Lian, Gene expression in the adipose tissue of NAFLD rats intervened with the extracts of polygonum caspidatum, J. Med. Res. 38 (2009) 54–57.
[16] Y.J. Wang, Y. Jin, F.J. Wang, F. Peng, Effect of Baohewan and Baohewan Added with Huzhang on Rats with Nonalcoholic Hepatosteatosis, 45 Acta. U. Med. Anhui, 2010, pp. 354–357.
[17] L.Q. Xu, Y.L. Xie, S.H. Gui, X. Zhang, Z.Z. Mo, C.Y. Sun, C.L. Li, D.D. Luo, Z.B. Zhang, Z.R. Su, J.H. Xie, Polydatin attenuates D-galactose-induced liver and brain damage through its anti-oxidative, anti-inflammatory and anti-apoptotic effects in mice, Food Funct. 7 (2016) 4545–4555.
[18] H. Zhang, C.H. Yu, Y.P. Jiang, C. Peng, K. He, J.Y. Tang, H.L. Xin, Protective effects of polydatin from polygonum cuspidatum against carbon tetrachloride-induced liver injury in mice, PLOS One 7 (2012) e46574.
[19] K. Huang, C. Chen, J. Hao, J. Huang, S. Wang, P. Liu, H. Huang, Polydatin promotes Nrf2-ARE anti-oxidative pathway through activating Sirt1 to resist AGEs-induced upregulation of fibronetin and transforming growth factor-beta1 in rat glomerular messangial cells, Mol. Cell. Endocrinol. 399 (2015) 178–189.
[20] L. Chen, Z. Lan, Polydatin attenuates potassium oxonate-induced hyperuricemia and kidney inflammation by inhibiting NF-kappab/NLRP3 inflammasome activation via the AMPK/SIRT1 pathway, Food Funct. 8 (2017) 1785–1792.
[21] L. Xue, K. Wu, H. Qiu, B. Huang, R. Chen, W. Xie, Q. Jiang, Polydatin exhibits the hepatoprotective effects through PPAR-α/-β signaling pathway in streptozocin-induced diabetic mice, J. Funct. Food 36 (2017) 341–347.
[22] J.M. Zhang, Y.Y. Tan, F.R. Yao, Q. Zhang, Polydatin alleviates non-alcoholic fatty liver disease in rats by inhibiting the expression of TNF-alpha and SREBP-1c, Mol. Med. Rep. 6 (2012) 815–820.
[23] L. Chen, Z. Lan, Q. Lin, X. Mi, Y. He, L. Wei, Y. Lin, Y. Zhang, X. Deng, Polydatin ameliorates renal injury by attenuating oxidative stress-related inflammatory responses in fructose-induced urate nephropathic mice, Food Chem. Toxicol. 52 (2013) 28–35.
[24] S.A. Polyzos, C.S. Mantzoros, Adiponectin as a target for the treatment of non-alcoholic steatohepatitis with thiazolidinediones: a systematic review, Metabolism 65 (2016) 1297–1306.
[25] D. Barb, P. Portillo-Sanchez, K. Cusi, Pharmacological management of nonalcoholic fatty liver disease, Metabolism 65 (2016) 1183–1195.
[26] K. Cusi, Treatment of patients with type 2 diabetes and non-alcoholic fatty liver disease: current approaches and future directions, Diabetologia 59 (2016) 1112–1120.
[27] X. Wang, D.M. Zhang, T.T. Gu, X.Q. Ding, C.Y. Fan, Q. Zhu, Y.W. Shi, Y. Hong, L.D. Kong, Morin reduces hepatic inflammation-associated lipid accumulation in high fructose-fed rats via inhibiting sphingosine kinase 1/sphingosine 1-phosphate signaling pathway, Biochem. Pharmacol. 86 (2013) 1791–1804.
[28] C. Tonelli, I.I.C. Chio, D.A. Tuveson, transcriptional regulation by Nrf2, Antioxid. Redox Signal. (2017) Epub.
[29] G. Marchesini, S. Petta, R. Dalle Grave, Diet, weight loss, and liver health in non-alcoholic fatty liver disease: pathophysiology, evidence, and practice, Hepatology 63 (2016) 2032–2043.
[30] G. Wu, L. Zhu, X. Yuan, H. Chen, R. Xiong, S. Zhang, H. Cheng, Y. Shen, H. An, T. Li, H. Li, W. Zhang, Britanin ameliorates cerebral ischemia-reperfusion injury by inducing the Nrf2 protective pathway, Antioxid. Redox Signal. 27 (2017) 754–768.
[31] X. He, Q. Ma, Redox regulation by nuclear factor erythroid 2-related factor 2: gatekeeping for the basal and diabetes-induced expression of thioredoxin-interacting protein, Mol. Pharmacol. 82 (2012) 887–897.
[32] Y. Hou, Y. Wang, Q. He, L. Li, H. Xie, Y. Zhao, J. Zhao, Nrf2 inhibits NLRP3 inflammasome activation through regulating Trx1/TXNIP complex in cerebral ischemia reperfusion injury, Behav. Brain Res. 336 (2018) 32–39.
[33] C.F. Lu, F. Zhang, W.X. Xu, X.F. Wu, N.Q. Lian, H.H. Jin, Q. Chen, L.Y. Chen, J.J. Shao, L. Wu, Y. Lu, S.Z. Zheng, Curcumin attenuates ethanol-induced hepatic steatosis through modulating Nrf2FXR signaling in hepatocytes, IUBMB Life 67 (2015) 645–658.
[34] L. Gou, L. Zhao, W. Song, L. Wang, J. Liu, H. Zhang, Y. Huang, C.W. Lau, X. Yao, X.Y. Tian, W.T. Wong, J.Y. Luo, Y. Huang, Inhibition of miR-92a suppresses oxidative stress and improves endothelial function by upregulating heme oxygenase-1 in db/db mice, Antioxid. Redox Signal. (2017) Epub.
[35] T.A. Kamalden, A.M. Macgregor-Das, S.M. Kannan, B. Dunkerly-Eyring, N. Khaliddin, Z.H. Xu, A.P. Fusco, S. Abu Yazib, R.C. Chow, E.J. Duh, M.K. Halushka, C. Steenbergen, S. Das, Exosomal microRNA-15a transfer from the pancreas augments diabetic complications by inducing oxidative stress, Antioxid. Redox Signal. 27 (2017) 913–930.
[36] G.Z. Wang, J.H. Yao, Z.L. Li, G. Zu, D.C. Feng, W. Shan, Y. Li, Y. Hu, Y.F. Zhao, X.F. Tian, miR-34a-5p inhibition alleviates intestinal ischemia/reperfusion-induced reactive oxygen species accumulation and apoptosis via activation of SIRT1 signaling, Antioxid. Redox Signal 24 (2016) 961–973.